

DYNAMICS OF AN EXPERIMENTAL TWO BLADED HORIZONTAL
AXIS WIND TURBINE WITH BLADE CYCLIC PITCH VARIATION*

Kurt H. Hohenemser and Andrew H. P. Swift

Washington University
St. Louis, Missouri 63130

ABSTRACT

The horizontal axis wind turbine under study incorporates the combination of two features: The application of blade cyclic pitch variation and the use of yaw angle control for rotor speed and torque regulation. Due to its "emasculatation" by passive cyclic pitch variation the rotor can be rapidly yawed without encountering gyroscopic and aerodynamic hub moments and without noticeable out-of-plane blade excursions. The two bladed upwind rotor is vane stabilized and of very simple and rugged design. The principle was first checked out with a small scale wind tunnel model and then tested in the atmosphere with a 7.6 meter diameter experimental fully instrumented wind turbine driving a 3 phase alternator. The rotor to tail vane furl angle was controlled through an electric actuator by a manually operated toggle switch overridden by an automatic rotor overspeed relay. The paper summarizes the test results with respect to structural dynamics and yaw dynamics.

A selection of subsequent power-on test results with emphasis on structural and yaw dynamics are given in this paper. Continued testing is planned for the spring of 1981.

THE NEW CONFIGURATION

In order to place the new configuration within the frame work of preceding designs, let us first look at the various possible ways of power and rotor speed control for horizontal axis machines.

Power and RPM Limitation By

1. Blade stall, automatic brake
2. Blade feathering
3. Blade Unfeathering (enhanced stall)
4. Rapid rotor yawing, cyclic pitch

The first method is applicable if an induction generator is used with nearly constant RPM imposed by the electric grid. At fixed blade pitch setting and increasing wind speed the rotor power will reach a maximum and then decline leading ultimately to deep blade stall. In case of power cut-out the rotor will overspeed unless speed limited by an automatic mechanical or aerodynamic brake. While this system is simple it requires an over designed generator and drive system and a powerful brake.

The second method is widely used and effective for both power-on and power-off conditions. It needs variable pitch blades and an automatic pitch control mechanism. The implementation of this method is complex and costly.

The third method enhances blade stall both power-on and power-off. The power peak remains high and requires an over designed generator and drive system. The blade pitch varying mechanism adds to the complexity and cost.

The fourth method of rapid rotor yawing using cyclic pitch variation is the one to be discussed here. Let us now look at the various possible means of generating a yawing moment.

Yawing Moment By

1. Yaw gear, up or downwind rotor
2. Tail vane, upwind rotor
3. Rotor control, up or downwind rotor
4. Rotor self yawing, downwind rotor

The first method is used in many medium and large units. The yaw rate is low so that the rotor position lags behind wind direction changes. In some designs the yaw gear drive is powered by a paddle wheel with an axis perpendicular to

NOMENCLATURE

A	Rotor disk area
A _T	Tail vane area
I _T	Machine moment of inertia about yaw axis
P	Rotor power
R	Rotor radius
T	Rotor Torque
V	Wind speed
C	Blade chord
C _{Lα}	Tail vane lift slope
C _P	Rotor power coefficient ($2P/\rho AV^3$)
C _Q	Rotor torque coefficient ($T/\rho AR(\Omega R)^2$)
α _Q	Rotor angle of attack
α _T	Tail vane orientation
α _{TO}	Instantaneous wind direction change at tail vane
ζ	Damping ratio
λ	Tip speed ratio ($\Omega R/V$)
ρ	Air density
σ	Blade solidity ratio ($2C_{\tau}/\pi R$)
τ	Cyclic pitch amplitude
Ω	Rotor angular speed
ω	Undamped natural yaw frequency
ω _n	Damped natural yaw frequency

INTRODUCTION

The bewildering variety of wind turbine configurations now in operation is a sign of a lack of maturity of this technology. In the course of time most of these configurations will undoubtedly fall by the wayside and only a few will survive. Meanwhile one more configuration of a horizontal axis wind turbine has been added and tested for several months in the atmosphere. Initial power-off test results are reported in Reference 1.

*Presented at the Second DOE/NASA Wind Turbine Dynamics Workshop, February 24-26, 1981 in Cleveland, Ohio.

the rotor axis. In other designs the yaw gear is driven by a servo motor receiving signals from wind direction pick-ups.

The second method is widely used for smaller units. Because of the gyroscopic and aerodynamic hub moments rapid wind following due to the tail vane can be a problem with respect to loads and vibrations, particularly for fast turning two bladed rotors. Our experimental wind turbine is tail vane stabilized and two bladed. It is subjected to high yaw rates. Due to the feature of passive cyclic pitch variation to be explained later, the rotor is "emasculated". Gyroscopic moments are balanced by aerodynamic moments from cyclic pitch variation and do not load up the hub or rotor shaft. The out-of-plane blade motions associated with the cyclic pitch variation are very small. There is no blade feathering mechanism.

The third method of yawing the rotor by active rotor cyclic pitch controls has been suggested in Reference 2 but has so far not been implemented.

The fourth method is limited to downwind rotors and has become quite popular. Its implementation requires a good understanding of rotor aerodynamics. Dynamic overshooting and large off-center equilibrium positions have been observed.

Figure 1 is a schematic plan view of the experimental wind turbine configuration with the definition of rotor angle of attack α , yaw angle $90^\circ - \alpha$ and furl angle. Though not quite correct, the furl angle, that is the angle between tail vane boom and rotor axis, has been assumed to be equal to the yaw angle. The furl angle could be varied between zero and almost 90° with the help of a linear electric actuator with a constant furl rate of 15 degrees per second. A toggle switch was used for starting, stopping and reversing the actuator motion. An automatic overspeed relay could override the manual switch in the direction of increasing furl angle. The actuator motion stopped when the overspeed condition terminated, or when the furl limit switch was tripped. Unfurling was then accomplished by manual operation of the toggle switch.

The 7.6 meter (25 foot) diameter turbine was driving a 3 phase alternator with a rectifier that produced up to 220 volt DC. A resistance load of 6.0 ohm resulted at 22 miles per hour wind velocity in an electric power output of 8.0 KW. The alternator torque input increases very closely with the second power of the RPM. Thus the wind turbine operated at all wind speeds and furl angles with a constant torque coefficient.

SMALL SCALE WIND TUNNEL MODEL STUDIES

The study of the new configuration began with some small scale wind tunnel model tests. Figure 2(a) shows an axial view of the model rotor. Figures 2(b) and 2(c) show side views. The hub can swivel freely about the two pins. The blades are attached to the hub with a small fixed prelag angle with respect to the swivel axis. The rotational deflection about the swivel axis is almost equal to the cyclic pitch deflection of the blade

pair which is accompanied by a small out-of-plane teeter deflection. Because of the absence of any control mechanism the hub is very simple. The blades are retained by bending flexures. Only autorotational conditions could be tested. The following table gives the main data for the wind tunnel model and for the atmospheric test machine.

Table 1

Model and Full Scale Parameters

	Model	Full Scale
Rotor Diameter inch	17.2	300
Blade Chord, inch	1.0	12 to 4
Blade Solidity Ratio	.075	.032(at .7R)
Blade Twist, degrees	0	9.5
Blade Airfoil, NACA	0015	4425 to 4412
Blade Lock Number	6.4	7.0
Blade Prelag Angle	23 ^o	23 ^o
Cyclic Pitch Stops	+9	+13 ^o
Reference Rotor RPM	1800	225
Reynolds Number for .7R	50,000	640,000

Since blade Lock number and blade prelag angle are approximately the same for model and full scale rotor, blade cyclic pitch dynamics are, outside of the blade stall regime, the same despite the differences in geometry. The measured quantities were wind speed, rotor speed and yaw angle. The furl angle (see Figure 1) could only be changed between runs and not during operation. The model was tested both with tail vane (Figure 2(b)) and without tail vane (Figure 2(c)) at fixed yaw angles. Figure 3 shows the speed ratio $V/\Omega R$ vs. yaw angle in autorotation for about zero blade pitch angle setting. The model data are corrected for a .7R Reynolds number of 50,000 since not all tests were run at this Reynolds number. The results of the full scale power-off tests at a Reynolds number of 640,000 are also shown. The dash line refers to the results of NACA tests at zero blade pitch setting and with a Reynolds number of 620,000, Reference 3. The NACA test results represent a smooth continuation of the curve for our atmospheric test rotor. The model, due to the lower Reynolds number and higher blade solidity, operates at much higher speed ratio $V/\Omega R$ and exhibits at 50° yaw angle a discontinuity in the curve, which is apparently caused by blade stall. The small scale model tests demonstrated smooth operation of the two bladed rotor with passive cyclic pitch variation up to yaw angles of 50 degrees, good controllability of the RPM by yawing, easy starting up to 50° yaw angle, good damping of yaw transients and the capability of high yaw rate without noticeable vibrations.

In the original configuration of the model rotor an instability occurred with zero yaw angle at a wind speed of 24 miles per hour corresponding to 2100 RPM. Just prior to the onset of the instability the cyclic pitch amplitude was small and the rotor ran smoothly. Suddenly cyclic pitch stop pounding was observed with an estimated frequency of 10 to 20 Hz. The RPM rapidly dropped to about one-third and the

tip path plane was strongly warped indicating that the cyclic pitch frequency was different from the usual 1P. The condition persisted until the tunnel speed was reduced to 12 miles per hour. The onset of the instability was, in repeated tests, always exactly at 24 miles per hour.

It was suspected that the instability was related to the fact that, for the model, the blade coning frequency was quite low due to the blade retention flexures. These flexures were reinforced in order to appreciably raise the blade coning frequency. The model was then operated at zero yaw angle up to 28 miles per hour wind speed corresponding to 2500 RPM without encountering the instability. At 28 miles per hour the model was yawed whereby the rotor speed dropped at 45 degrees yaw angle to 1450 RPM. When yawing further beyond 50 degrees the stop pounding instability reoccurred but could be removed by yawing the rotor back to smaller yaw angles. The observed effect of the coning mode frequency on the instability proves that a coupling between the rigid body blade mode and the coning mode is involved. Blade stall must also be a contributor, otherwise the two modes could not couple, the coning mode being symmetrical, the rigid body mode being asymmetrical. The full scale rotor was tested up to 36 miles per hour wind speed and up to 80 degrees yaw angle without encountering the instability. Presumably it was not stalled in this test range. The coning frequency is high, see Figure 8.

The model instability may be related to a phenomenon observed with the NASA DOE MOD-0 machine in the configuration with teetering untwisted blades reported in Reference 4. The MOD-0 operated for these tests at substantially lower RPM than normal and closer to blade stall. Stop pounding of the teetering motion occurred repeatedly after encountering a gust. The stop pounding condition persisted after passing of the gust and could only be removed by feathering the blades. Stop pounding has also occurred in two bladed teetering helicopter rotors and has caused the destruction of rotors in flight. Conditions with deep stall should be avoided in teetering rotors.

ANALYSIS OF STEADY STATE YAW CHARACTERISTICS

The analytical studies were conducted in support of the design for the atmospheric test equipment. Figure 4 shows the effect of yaw angle on the power coefficient C_p . The curves are labelled according to the rotor angle of attack (90° minus yaw angle, see Figure 1). The graphs have been estimated with the method of Reference 5, correcting for the opposite blade twist and for dynamic stall effects. Similar graphs based on analysis are given in Reference 6, based on tests in Reference 7. The cubic curve $C_p/\sigma = .008$ represents approximately the power required coefficient for the 3 phase alternator. The operational points for the various yaw angles, indicated by circles, are the intersections of the power required and power available curves. At zero yaw angle ($\alpha = 90^\circ$) the machine operates with maximum power coefficient. The tip speed ratio $\Omega R/V$ is constant up to rated wind speed, the RPM then varies in proportion to the wind speed. Beyond

rated wind speed the RPM and power is kept constant by yawing the wind turbine out of the wind. The power coefficient is now smaller and less than the maximum for a given yaw angle.

ANALYSIS OF YAW TRANSIENTS

Yaw transients are easy to compute since one can assume that the emasculated rotor does not resist a yawing motion. The undamped natural frequency in yaw depends only on the tail vane parameters.

$$\omega = (C_{L\alpha} q A_T h / I)^{1/2}$$

The yaw damping ratio is

$$\zeta = \omega h / 2V$$

The natural frequency of the damped yawing motion is

$$\omega_n = (1 - \zeta^2)^{1/2}$$

For the test machine: $A_T = 12.5 \text{ ft}^2$, $C_{L\alpha} = 3.0$, $I = 370 \text{ slug ft}^2$, $h = 15.5 \text{ ft}$. A wake factor of .7 was assumed to obtain the lift slope. For $V = 21 \text{ miles per hour (9.5 meter per second)}$ and standard sea level density one obtains

$$\omega_n = 1.31 \text{ rad/s}, \zeta = .33$$

The yaw response to a unit step input of wind direction change is shown in Figure 5. The new wind direction is reached after 1.5 seconds and there is a 30% overshoot. After 4 seconds the machine is practically aligned with the new wind direction and stays aligned. The maximum yaw rate is $.6\alpha \tau_0 \text{ rad/sec}$.

It is of interest to establish the effect of upscaling of the machine. From the given expressions it follows for geometric similarity and assuming that masses increase with the cube of the length dimension:

- o The natural yaw frequency increases in proportion to wind speed.
- o The natural yaw frequency is inversely proportional to the length dimension.
- o The yaw damping ratio is independent of wind velocity and of scale.
- o The damping ratio increases with $h(hA_T/I)^{1/2}$. For given geometry a light tail boom gives a high damping ratio.

One can easily show that for the rotor, assuming the cube law for the masses, the natural frequencies are also inversely proportional to the length dimension, and that damping ratios are independent of scale. Thus, the rotor scaling laws match those for the tail vane. A given step change in wind direction will lead, at the same wind speed, to the same cyclic pitch amplitude, no matter what the scale. Figure 5 shows also the time scale for a MOD-OA size machine with 5 times the diameter of the test rotor.

FURL TEST DATA

A number of power-off and power-on furling tests were conducted and several automatic furlings occurred in response to rotor overspeed. A particularly severe furling test consisted of a sudden power cut with simultaneous start of furling as it could occur by the blowing of a fuse in the alternator load circuit. Figure 6 shows the time history for such a case. The initial conditions were 16.5 miles per hour wind speed, 170 rotor RPM, 15° furl angle. The furl angle reached its maximum value of 80° after 4.3 seconds (15°/sec). The rotor speed reached the maximum of 225 RPM after 3.3 seconds. After 8 seconds a gust occurred increasing the wind speed to 20 miles per hour. At the same time the power was inadvertently cut in for 2 seconds. The RPM declined steadily. The overspeed ratio for this power cut-out case was 225/170 = 1.32. The rotor, the transmission system and the generator must be capable of occasionally sustaining such an overspeed. If the power cut-out should happen together with the beginning of a gust, the overspeed would be greater. A higher furl rate than 15°/sec would reduce the overspeed after power cut-out. The wind velocity was measured at 45 feet height, 15 feet below the rotor center.

VIBRATIONS AND DYNAMIC LOADS TEST DATA

The test machine is a modified Astral Wilcon Model 10B mounted on a free standing Unarco-Rohn S.S.V. 60 foot high tower which has been made tiltable to a near horizontal position to facilitate maintenance of the instrumentation. Vibration frequencies and damping ratios were first analyzed and then corrected from vibration test results at zero rotor speed. The effect of rotor speed on the blade natural frequencies as shown in Figures 7 and 8 was computed. The operational range is between 120 and 250 RPM. In this range there is a 3P resonance with the fundamental in-plane rotor mode. It was found to be hardly noticeable. The 2P coning mode resonance at an overspeed of 280 RPM is quite strong despite a high damping ratio of .21. Higher harmonic resonances with the higher modes were found to be weak. There is a wide separation between the in-plane mode frequency and the 1P line. The 1P gravity excitation is, therefore, not amplified and no 2P gravity hub loads exist. The asymmetrical rigid body mode (cyclic pitch) is placed between the 1P and 3P lines and shows little resonance excitation. This mode is furthermore well damped with a damping ratio of .26.

Of the various tower and tail boom modes only the 3 modes listed in Table 2 were found to be of any significance.

Table 2

Tower and Tail Boom Resonances

Excitation	First Tower	Vertical Boom	Second Tower
1P	112	160	--
2P	56	80	--
4P	28	40	180

The 1P tower excitation at 112 RPM was found to be mild. There is a 1P vertical tail boom excitation at 160 RPM which has an effect on almost all dynamic loads as seen in Figure 9, where the main harmonic contents is indicated for each graph. The yaw post bending moment is taken at the upper yaw bearing and peaks at the vertical tail boom 1P resonance of 160 RPM. The tail boom vertical root moment, not shown in Figure 9, is equal to the yaw post moment. It appears that the vertical tail boom resonance affects, in addition to the yaw post, also the blades. The stresses from these loads are quite small. The vertical and horizontal accelerations of the machine just aft of the hub are also small, not exceeding ±.15g even at the tower or tail boom resonances.

Table 3 shows the maximum measured dynamic transient loads at 3 furl angles for yaw post bending, for flap bending of the rotor center, and for rotor torque. The 1P in-plane bending amplitude at the rotor center is constant throughout and determined by gravity loads. Despite the two bladed rotor and despite rapid yawing the test machine is quite benign with respect to dynamic loads and vibrations.

Table 3

Maximum Transient Loads + in-lbs

Furl Angle	RPM	Yaw Post	Flap Bend.	Torque
15°	200	4100	2500	1170
30°	200	3500	3100	1160
45°	144	3700	440	670

In-plane bending: 1800 in-lbs throughout

Analyses for several potential linear aeroelastic instabilities were performed. Bending torsion blade flutter up to 400 RPM cannot occur. A whirl instability of the two bladed rotor is predicted for equal rotor support stiffness in the vertical and horizontal direction. Due to the free yawing the horizontal rotor support stiffness is zero and analysis as well as tests showed that in this case no whirl instability exists. The Coleman type of mechanical instability from coupling of the in-plane blade mode with the rotor support mode was analyzed and found to occur far above 400 RPM. The rotor rigid body mode frequency coalesces with the in-plane mode frequency at about 350 RPM. A closed form approximate solution showed a slight negative damping ratio of the coupled mode. A more elaborate finite element analysis resulted in positive damping of this mode. One can conclude that the test machine is free of linear aeroelastic instabilities.*

STARTING TEST DATA

The wind velocity required for starting depends on the system friction torque and on the aerodynamics of the inner blade section. Due to

*The aeroelastic and vibration analyses were performed by the graduate students T.W.H. Ko and S.Y. Chen, under the supervision of Professor D.A. Peters.

the feathering mechanism of the Astral Wilcon Model 10B machine, 30% of the inner blade has no aerodynamic section but merely a circular shaft. Though the test rotor has no feathering mechanism and could have an aerodynamic section extending close to the hub, the available Model 10B blades were used to keep the cost of the test machine low.

Figure 10 shows a comparison of the test blade planform with a possible planform of a production blade, which would have, according to the analysis, twice the starting torque and a considerably improved performance. The measured contributions to the starting rotor torque were:

Rotor shaft and gearbox	3.5 foot lbs.
Alternator	1.0 foot lbs.
Alternator belt drive	1.0 foot lbs.
Total	5.5 foot lbs.

Figure 11 shows the time history of a starting test less belt drive, that is with 3.5 foot lbs. starting friction. The production type blade would have about the same characteristics with 7 foot lbs. starting friction. With 8 miles per hour average wind velocity the rotor accelerates steadily to 40 RPM within 40 seconds. It then takes off very rapidly and reaches 120 RPM in another 10 seconds. The cyclic pitch amplitude is initially large with an occasional stop contact at $+11.5^\circ$ during the first few revolutions. Beyond 40 RPM the amplitude reduces to a small value of $+2^\circ$. Starting tests were conducted up to a furl angle of 60° . Somewhat higher wind velocity is required for starting at higher furl angles.

STATISTICAL TEST DATA

Due to the fluctuating wind velocities it is difficult to obtain data on steady conditions. The data points in Figure 12 of rotor power vs. rotor speed were obtained during brief periods of approximately steady wind. For both unfurled and 40° furl conditions the data follow closely the constant torque coefficient line $C_p/\sigma = .008$, see also Figure 4. The highest two points were taken during gusts when the rotor was accelerating. The power from the torque meter reading was corrected for the accelerating torque. The total torque including the inertia torque is again on the $C_p/\sigma = .008$ line.

The statistical data presented in Figures 13 to 18 were obtained with a microcomputer. For each dynamic variable 128 samples per second were taken. The computer then updated mean, standard deviation, overall maximum and overall minimum. After completing this task for all measured variables, the next set of 128 samples per second per quantity was taken. The intervals between the sample sets were about 3 seconds. For each sample set of one second duration the wind velocity was measured and the 1/2 meter per second wide velocity "bin" was determined for that particular set. Each run lasted for about one hour.

Figure 13 shows a typical distribution of sample sets. A logarithmic scale is used for the number of sample sets. Each wind speed "bin" between 2 and 6 meter per second contains about 100 sample

sets, whereby each set contains 128 samples per measured quantity. The average power coefficient for each bin is shown in Figure 14. At low wind speed this coefficient is high because the inertia of the decelerating rotor adds to the shaft torque. At high wind speed the power coefficient is low because the inertia of the accelerating rotor subtracts from the shaft torque, see also Figure 12. If one weighs the average C_p value in each wind speed bin with the number of sample sets in this bin, and if one then takes the weighted average over all bins, one obtains the value of $C_p = .46$. This represents the ratio of the energy transmitted during the run to the shaft over the total wind energy flowing through the disk during the period of the run.

Figure 15 shows the distribution of the average power coefficient for 45° furl angle. The C_p values are now much lower, the weighted average over all bins is $C_p = .18$.

Figure 16 shows an example of the distribution of mean and standard deviation of the rotor RPM over the bins. For steady conditions the tip speed ratio λ should be independent of wind speed. Actually the tip speed ratio is higher at low wind speed, because the rotor runs faster than for equilibrium, the tip speed ratio is lower for high wind speed, when the rotor runs slower than for equilibrium.

Figure 17 shows an example of the mean, standard deviation, maximum and minimum of the cyclic pitch amplitude vs. rotor RPM "bins" at 30° furl angle. The vertical scale is in volt, whereby 1 volt = 5° cyclic pitch amplitude. For low RPM the mean cyclic pitch amplitude is $+5^\circ$, for higher RPM it is about $+2.5^\circ$.

Figure 18 shows an example of the effect of yaw rate on the cyclic pitch amplitude. Yaw rate "bins" of 3°/sec. width were used and the mean and standard deviation of the cyclic pitch amplitude in each bin was determined. For the case of Figure 18 the furl angle was 20° , and the yaw rates were obtained from the yaw post rotation due to wind direction changes. Only yaw rates in the furl direction were considered. For the opposite yaw rates the cyclic pitch amplitudes are about 30% smaller. A 14°/sec. yaw rate produces a mean cyclic pitch amplitude of $+4^\circ$ which is in agreement with analytical estimates.

CONCLUSIONS

The test data taken with the experimental wind turbine during close to 100 hours of operation in winds up to 36 miles per hour have shown that the two bladed vane stabilized rotor with passive cyclic pitch variation can be continuously operated power-on at yaw angles up to 50° with a low level of dynamic loads and vibrations. The machine can also be rapidly yawed with rates or more than 15°/sec without a noticeable increase in dynamic loads and vibrations. In partially furled conditions the rotor power can be held to a small fraction of the power when unfurled. With the present furl rate of 15°/sec

a sudden power loss results in 32% overspeed. So far automatic operation of the furl control was limited to overspeed furling. A fully automatic furl control is being developed.

REFERENCES

1. Hohenemser, Kurt H, and Swift, Andrew H.P., "The Yawing of Wind Turbines with Blade Cyclic Pitch Variation", SERI Second Wind Energy Innovative Systems Conference, December 3-5, 1980, SERI/CP-635-938, pp. 207-224.
2. Hohenemser, Kurt H., "Some Alternative Dynamic Design Configurations for Large Horizontal Axis WECS", Wind Turbine Structural Dynamics, Workshop held at Lewis Research Center, Cleveland, Ohio, November 1977, DOE CONF-771148.
3. Wheatley, J. B., and Bioletti, C., "Wind Tunnel Tests of 10 Foot Diameter Autogiro Rotors", NACA Report No. 552, October 1935.
4. Glasgow, J. C., and Miller, D. R., "Teetered Tip Controlled Rotor: Preliminary Test Results from MOD-O 100-KW Experimental Wind Turbine", AIAA/SERI Wind Energy Conference, April 9-11, 1980, Boulder, Colorado, pp. 261-268.
5. Gessow, A., and Tapscott, R. J., "Tables and Charts for Estimating Stall Effects on Lifting Rotor Characteristics", NASA TN D-243, May 1960.
6. Norton, J. H. Jr., "The Development and Testing of a Variable Axis Rotor Control System with 5 Meter Rotor and Direct Drive Alternator", Proceedings Small Wind Turbine Systems 1979 Workshop coordinated by Rockwell International and held at Boulder, Colorado, February/March 1979, Vol. 1, pp. 31-64.
7. Stoddard, F., Perkins, F., and Cromack, D., "Wind Tunnel Tests for Fixed-Pitch Start-up and Yaw Characteristics", Technical Report UM-WT-TR-78-1, NASA Lewis, June 1978.

The work was sponsored by the Solar Energy Research Institute in Golden, Colorado under Subcontract No. XH-9-8085-3 to Washington University Technology Associates (WUTA).

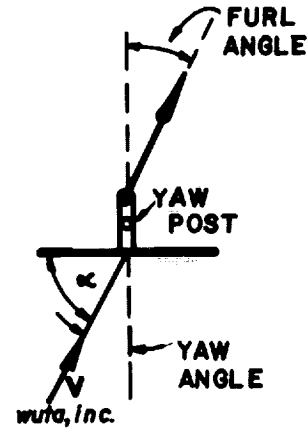


Figure 1—Schematic plan view

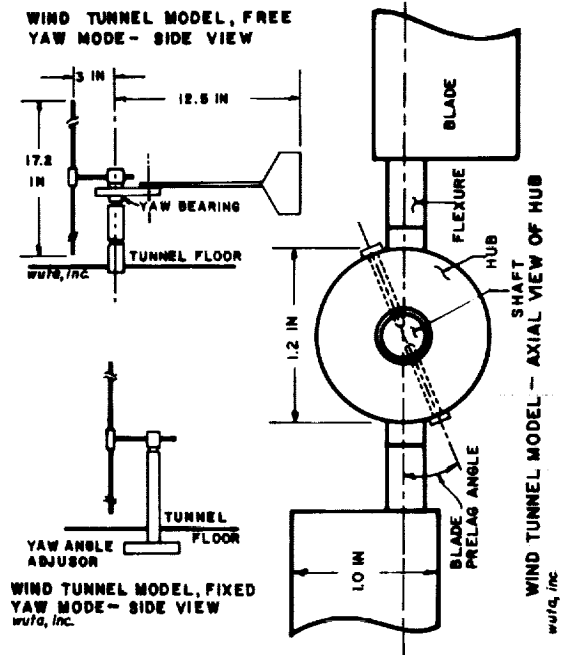


Figure 2—Wind tunnel model, (a) Axial view of hub, (b) Free yaw mode—side view, (c) Fixed yaw mode—side view.

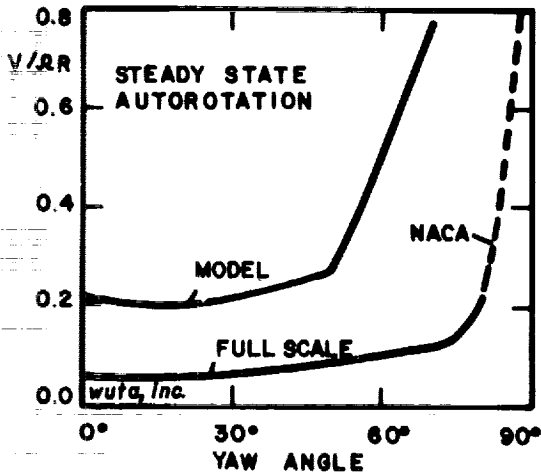


Figure 3— Test results, steady state model and full scale autorotation.

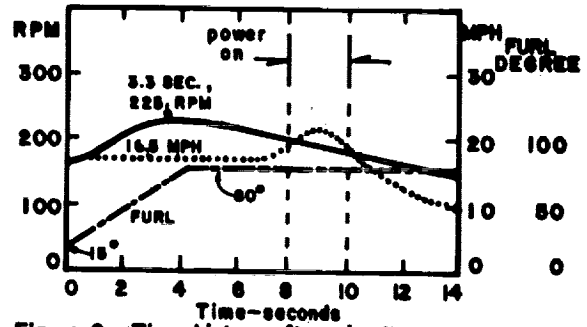


Figure 6— Time history after simultaneous power cut and initiation of furling.

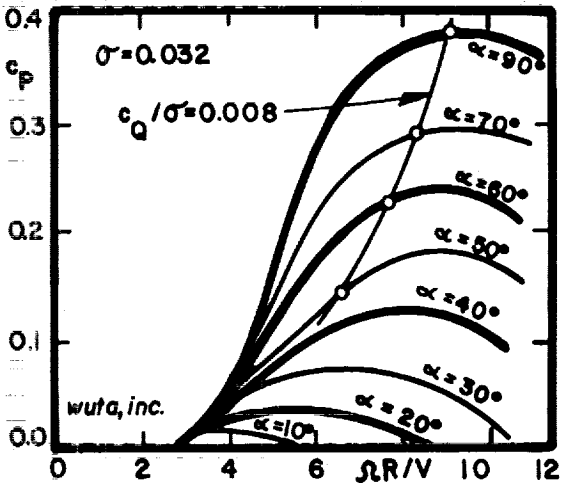


Figure 4— Power coefficient c_p vs tip speed ratio $\Omega R/V$ for constant rotor angle of attack values α .

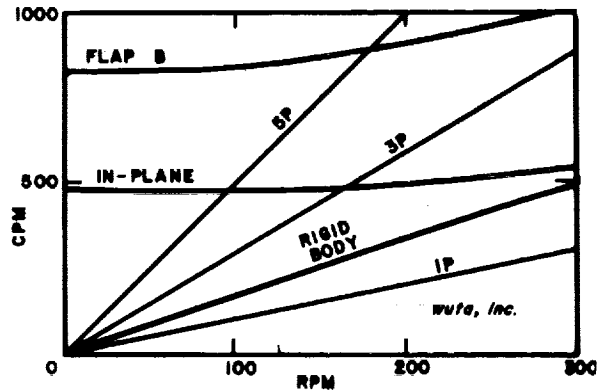


Figure 7— Asymmetrical rotor mode frequencies.

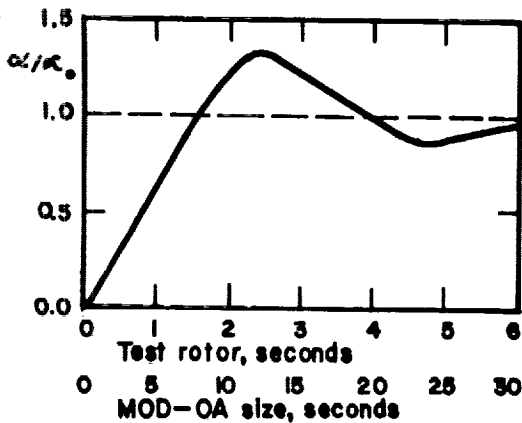


Figure 5— Yaw response to unit step input.

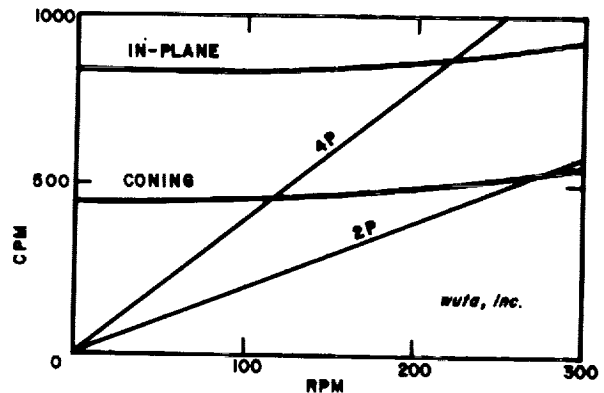
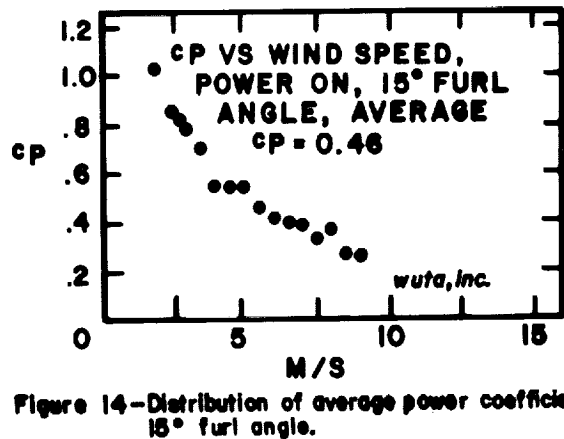
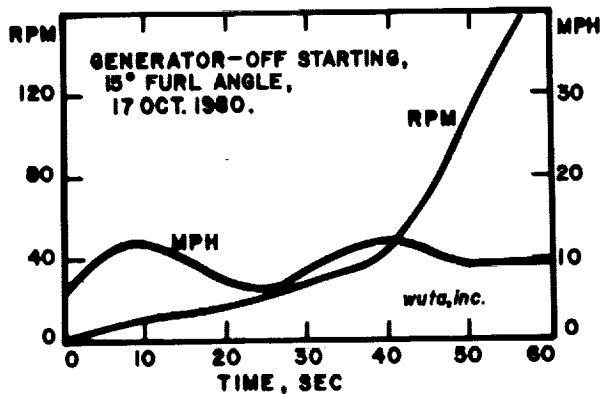
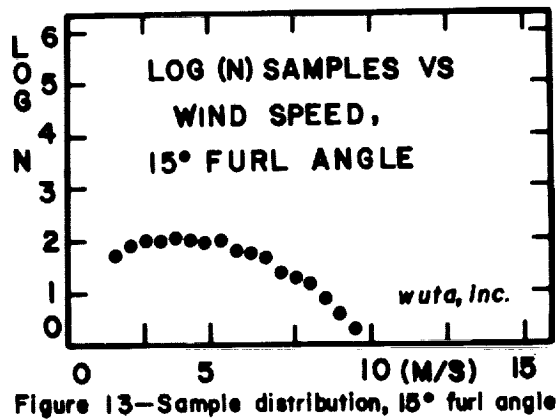
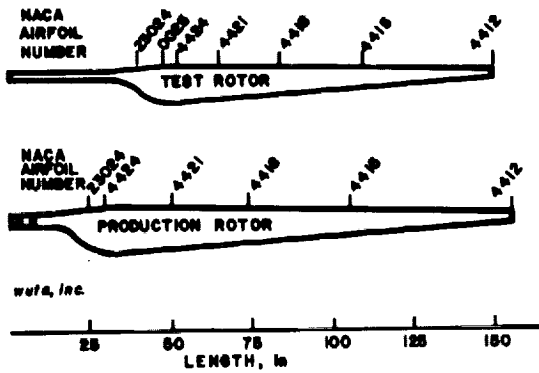
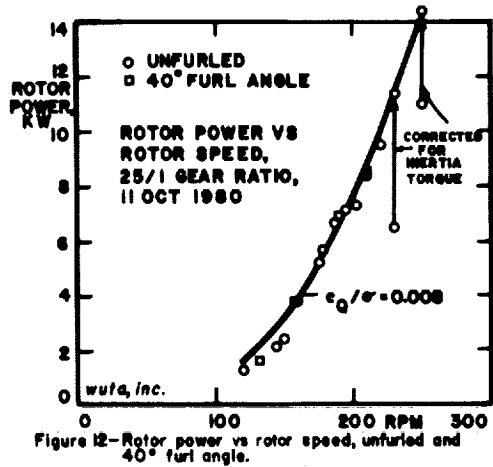
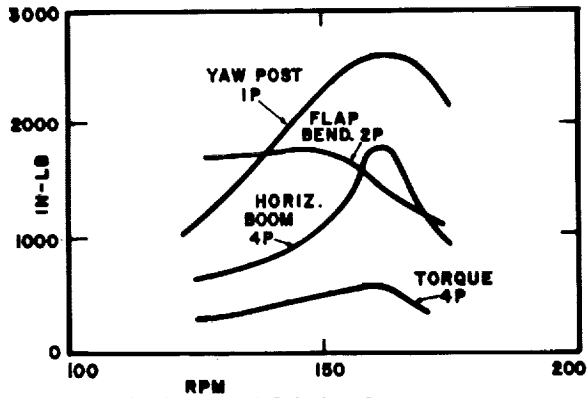


Figure 8— Symmetrical rotor mode frequencies.



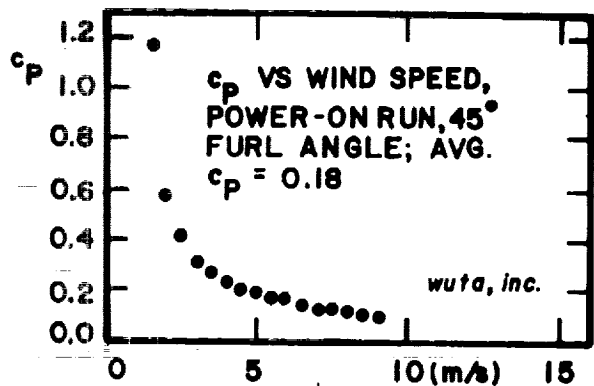


Figure 15—Distribution of average power coefficient, 45° furl angle.

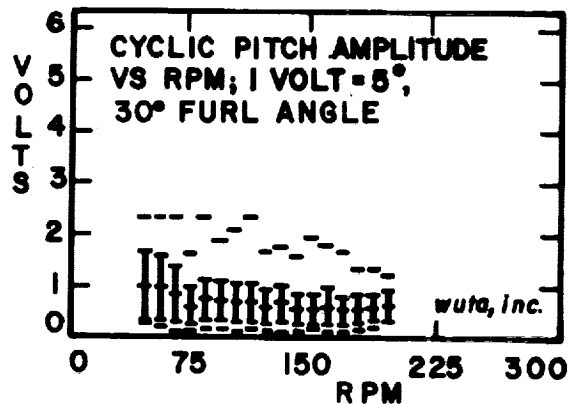


Figure 17—Pitch amplitude vs rotor RPM, 30° furl angle.

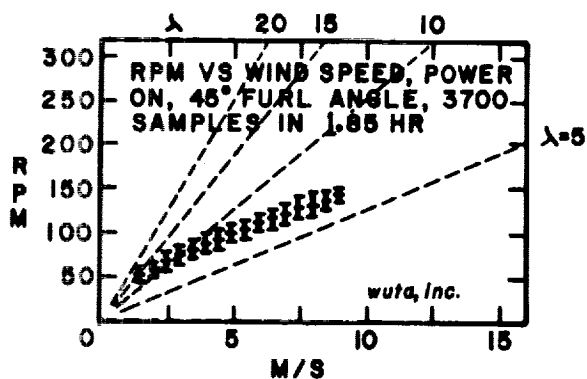


Figure 16—Rotor RPM distribution, 45° furl angle.

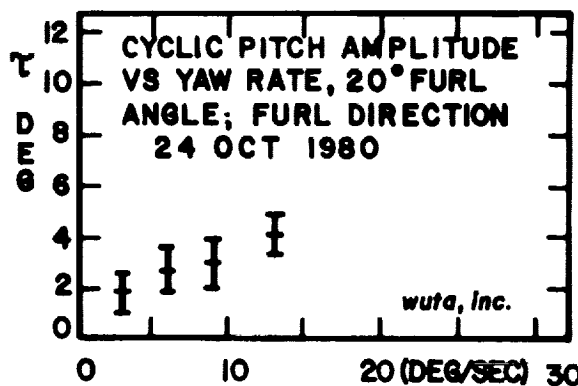


Figure 18—Cyclic pitch amplitude vs yaw rate, 20° furl angle.

QUESTIONS AND ANSWERS

K. Hohenemser

From: A. Smith

Q: Why such high $\Delta 3$ angles? And is the high rigid body frequency due to $\Delta 3$?

A: $\Delta 3$ has been selected to place the frequency of the rigid body mode between 1 P and 3 P. This gives a $\Delta 3$ of about 20° .